European Conference on Computational Fluid Dynamics
ECCOMAS CFD 2006
P. Wesseling, E. Oñate and J. Périaux (Eds)


# FLOODING AND DRYING IN DISCONTINUOUS GALERKIN DISCRETIZATIONS OF SHALLOW WATER EQUATIONS

**Vijaya R. Ambati***

*University of Twente, Department of Applied Mathematics
Ravelijn, 7500 AE Enschede, The Netherlands
e-mail: v.r.ambati@math.utwente.nl
web page: http://www.math.utwente.nl/∼ambativr/

**Key words:** Flooding and Drying, Front Tracking, Discontinuous Galerkin, Finite Element Methods

**Abstract.** *Accurate modeling of flooding and drying is important in forecasting river floods and near-shore hydrodynamics. We consider the space-time discontinuous Galerkin finite element discretization for shallow water equations with linear approximations of flow field. In which, the means (zeroth order approximation) is used to conserve the mass and momentum, and the slopes (first order approximation) are used to capture the front movement accurately in contrast to the finite volume schemes, where the slopes have to be reconstructed. As a preliminary step, we specify the front movement from some available exact solutions and show that the numerical results are second order accurate for linear polynomials. To resolve the front movement accurately in the context of discontinuous Galerkin discretizations, the front tracking and the front capturing methods are currently under investigation.*

## 1 INTRODUCTION

In the geophysical fluid dynamics, the nonlinear shallow water equations are generally used in the prediction of river floods and near-shore hydrodynamics. In many of these situations, a part of the boundary of the flow domain consists a free boundary where the water depth is zero. Due to the movement of this free boundary (or water front line) over a topography, flooding and drying events occur. Numerical modeling of flooding and drying in the space-time discontinuous Galerkin (DG) finite element discretizations of shallow water equations is the subject of the present paper.

Space-time DG finite element method for shallow water equations is first presented in Ambati and Bokhove [6] for fixed grids and subsequently extended it to dynamic grids in Ambati and Bokhove [7]. Now, it remains to predict the free boundary movement satisfying the zero water depth condition at the free boundary. Two approaches are

currently under investigation for prediction of the free boundary movement. The first approach is to use a front equation obtained by assuming that the water front line is single valued in either one of the horizontal co-ordinate directions and by applying a kinematic boundary condition. The second approach is to use a level set equation, where the level set demarcates the wet and regions with positive and negative values, respectively. As a preliminary step, we have specified the free boundary movement for some available exact solutions and obtained the numerical results. The zero water depth condition at these free boundaries are achieved by constraining the slopes in the finite elements connected to the free boundary.

First, we simulated the linear harmonic shallow water waves generated by a harmonic wave maker with our nonlinear numerical scheme. We observed that under low amplitude of the wave maker, the harmonic waves generated agrees with the exact solution under high amplitude these harmonic waves tend to break due to non-linearity. Second, we have tested the run-up and backwash on a parabolic beach, for which an exact solution is given in Thacker [**?**]. Similarly, we tested the dam break problem initialized with the exact solution after some time to avoid discontinuities in the solution. The method gives second order accurate results in space and time.

The paper is organized as follows: the shallow water and water front equations are introduced in §2. Space-time discontinuous Galerkin method is presented in §3. Modeling approach of flooding and drying is discussed in §4. Preliminary numerical results are presented in §5 and conclusion are drawn in §6.

## 2 SHALLOW WATER AND FREE BOUNDARY DYNAMICS

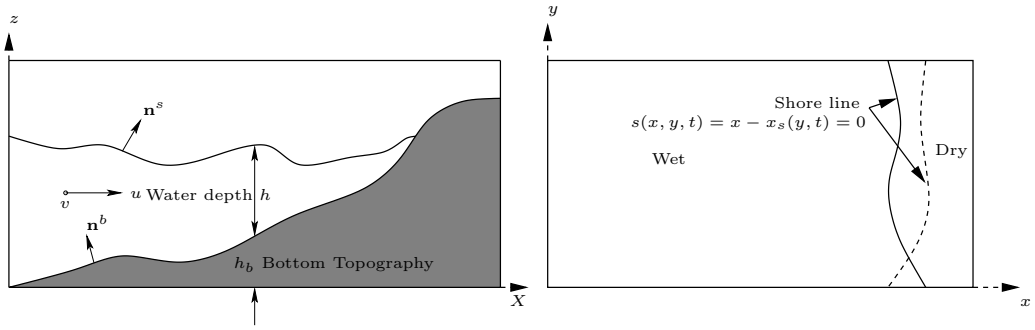


Figure 1: Typical cross section (left) and domain (right) of a beach.

The shallow water equations in the conservative form can be concisely given as

$$\nabla \cdot \mathcal{F}_i(\mathbf{U}) = S_i \text{ on } \mathbf{x} \in \Omega_f \tag{1}$$

with $\Omega_f$ the wet flow domain, $\mathbf{x} = (t, x, y)$ the coordinates, $\nabla = (\partial_t, \partial_x, \partial_y)$ the differential

operator, $\mathbf{U} = (h, hu, hv)$ the state vector,

$$\mathcal{F}_i(\mathbf{U}) = \begin{pmatrix} h & hu & hv \\ hu & hu^2 + gh^2/2 & huv \\ hv & huv & hv^2 + gh^2/2 \end{pmatrix} \tag{2}$$

the flux vector, $S_i = (0, -gh\partial_x h_b, -gh\partial_y h_b)$ the source vector, $h(\mathbf{x})$ the water depth, $\mathbf{u}(\mathbf{x}) = (u(\mathbf{x}), v(\mathbf{x}))$ the velocity field, $h_b(x, y)$ the bottom topography and $g$ the gravitational acceleration. The boundary $\partial\Omega_f$ is usually a combination of fixed boundaries $\Gamma_F$ and free boundaries $\Gamma_S$ ($\partial\Omega_f = \Gamma_F \bigcup \Gamma_S$). The system (1) can be completed with boundary conditions at fixed boundaries $\Gamma_F$ as inflow, outflow or solid wall boundary conditions; and at free boundaries as zero water depth $h = 0$. However, it is not trivial to determine the position of free boundary by solving system (1) and hence we consider the following two approaches:

- The position of free boundary $\Gamma_S$ can be determined by applying a kinematic boundary condition at the free boundary $\Gamma_S$ as

$$\partial_t s + (\mathbf{u} \cdot \bar{\nabla}) s = 0 \text{ at } \mathbf{x} \in \Gamma_S, \tag{3}$$

  where $\bar{\nabla} = (\partial_x . \partial_y)$ the space differential operator and $s(\mathbf{x}) = 0$ describes the free boundary curve $\Gamma_S$. As shown in Figure 1, we can assume the free boundary to be single valued *w.r.t.* $y-$axis such that $s(\mathbf{x}) = x - x_s(y, t) = 0$ and the equation (3) simplifies to

$$\partial_t x_s + v\partial_y x_s = u \text{ at } \mathbf{x} \in \Gamma_S, \tag{4}$$

  where $x_s(y, t)$ is the position of water from $y - axis$. This approach is applicable to restricted situations like run-up and backwash on beaches without forming dry islands.

- A general approach to determine the position of free boundary is the level set equation (Osher and Fedkiw [5]),

$$\partial_t \phi + (\mathbf{u} \cdot \bar{\nabla}) \phi = 0 \text{ at } \mathbf{x} \in \Omega, \tag{5}$$

  where $\Omega$ is a fixed domain consisting both the wet flow domain $\Omega_f$ and dry domain $\Omega_d$ ($\Omega = \Omega_f \cup \Omega_d$) and $\phi(\mathbf{x})$ the level set. The level set $\phi(\mathbf{x})$ demarcates the wet and dry regions of the domain with $\phi > 0$ and $\phi < 0$, respectively. However, to solve the level set equation (5) on $\Omega$, we have to define the extension velocities $\mathbf{v}_e$ in the dry domain $\Omega_d$ to replace $\mathbf{u}$ with $\mathbf{v}_e$ when $\phi < 0$ (see Sollie [8]).

## 3 SPACE-TIME DISCONTINUOUS GALERKIN METHOD

Space-time DG method of Ambati and Bokhove [7] will be summarized in this section. At first, we tessellate the space-time computational domain with space-time elements $\mathcal{K}_{\mathsf{k}}^n$ which are obtained by connecting the spatial elements in the time interval $I_n = [t_n, t_{n+1}]$. Each space-time element $\mathcal{K}_{\mathsf{k}}^n$ is mapped to a reference element $\hat{\mathcal{K}}$ by defining a mapping $G_{\mathcal{K}}^n : \hat{\mathcal{K}} \rightarrow \mathcal{K}_{\mathsf{k}}^n : \zeta \rightarrow \mathbf{x}$, where $\zeta = (\zeta_0, \zeta_1, \zeta_2)$ are the co-ordinates of the reference element $\hat{\mathcal{K}}$. Next, we define the finite element function space as:

$$\mathcal{V}_{\mathsf{h}}^d := \Big\{ \mathbf{V}_{\mathsf{h}} \in L^1(\mathcal{K}^n) \Big| \mathbf{V}_{\mathsf{h}}|_{\mathcal{K}} \in (P^1(\mathcal{K}))^d \Big\} \tag{6}$$

with $P^1$ the space of linear polynomials, $d = \dim(\mathbf{V}_{\mathsf{h}})$ and $\mathbf{V}_{\mathsf{h}}$ the polynomial approximation defined as $\mathbf{V}_{\mathsf{h}} := \sum_{m=0}^{M-1} \hat{\mathbf{V}}_m \psi_m$ with $\hat{\mathbf{V}}_m$ the expansion coefficients, $\psi_m$ the polynomial basis functions and $M$ the number of basis functions. The polynomial basis functions are first defined on reference element $\hat{\mathcal{K}}$ as

$$\hat{\phi}_m : \hat{\mathcal{K}} \rightarrow \mathbb{R} := \{1,\ \zeta_0,\ \zeta_1,\ \zeta_2,\ \zeta_1\zeta_2,\ \zeta_0\zeta_1,\ \zeta_2\zeta_0,\ \zeta_0\zeta_1\zeta_2\}, m = 0, \ldots, 7, \tag{7}$$

and then transformed onto each space-time element $\mathcal{K}_{\mathsf{k}}^n$ as $\phi_m : \mathcal{K}_{\mathsf{k}}^n \rightarrow \mathbb{R}$. $G_{\mathcal{K}}^n$. We either take $M = 5$ for fixed meshes or $M = 8$ for dynamic meshes. To split the polynomial approximation into element means $\hat{\mathbf{V}}_0$ and slopes $\hat{\mathbf{V}}_m$; $m = 1, \ldots, (M-1)$; we define the basis functions $\psi_m$ as

$$\psi_m(\mathbf{x}) : \mathcal{K}_{\mathsf{k}}^n \rightarrow \mathbb{R} := \begin{cases} 1 & m = 0 \\ \phi_m(\mathbf{x}) - \frac{1}{|K_{\mathsf{k}}^n|} \int_{K_{\mathsf{k}}^n} \phi_m(t_n^-, \bar{\mathbf{x}})\, \mathrm{d}K & \text{otherwise.} \end{cases} \tag{8}$$

Since the polynomial approximation $\mathbf{V}_{\mathsf{h}}$ is discontinuous at the finite element boundaries, we define the trace of the function $\mathbf{V}_{\mathsf{h}}$ on the element boundary $\partial\mathcal{K}_{\mathsf{k}}^n$ as

$$\mathbf{V}_{\mathsf{h}}(\mathbf{x})|_{\partial\mathcal{K}_{\mathsf{k}}^n} = \mathbf{V}^- := \lim_{\epsilon \uparrow 0} \mathbf{V}_{\mathsf{h}}(\mathbf{x} - \epsilon \mathbf{n}_{\mathcal{K}}) \tag{9}$$

with $\mathbf{n}_{\mathcal{K}}$ as the outward unit normal vector of the boundary $\partial\mathcal{K}_{\mathsf{k}}^n$.

The discontinuous Galerkin weak formulation can now be obtained by multiplying (1) with the test function $\mathbf{W}_{\mathsf{h}} \in \mathcal{V}_{\mathsf{h}}^d$ and integrating on each space-time element $\mathcal{K}_{\mathsf{k}}^n$: *Find a* $\mathbf{U}_{\mathsf{h}} \in \mathcal{V}_{\mathsf{h}}^d$ *such that for all* $\mathbf{W}_{\mathsf{h}} \in \mathcal{V}_{\mathsf{h}}^d$

$$\int_{\partial\mathcal{K}_{\mathsf{k}}^n} \mathbf{n}_{\mathcal{K}} \cdot \Big( W_i^- \tilde{\mathcal{F}}_i(\mathbf{U}^-, \mathbf{U}^+, \mathbf{n}_{\mathcal{K}}) \Big) \mathrm{d}(\partial\mathcal{K}) - \int_{\mathcal{K}_{\mathsf{k}}^n} \nabla W_{\mathsf{h}i} \cdot \mathcal{F}_i(\mathbf{U}_{\mathsf{h}})\, \mathrm{d}\mathcal{K} - \int_{\mathcal{K}_{\mathsf{k}}^n} W_{\mathsf{h}i}\, S_i\, \mathrm{d}\mathcal{K} = 0 \tag{10}$$

*is satisfied.* Note that, $\tilde{\mathcal{F}}_i(\mathbf{U}^-, \mathbf{U}^+, \mathbf{n}_{\mathcal{K}})$ is the numerical flux, which directly depends on the discontinuous traces of $\mathbf{U}_{\mathsf{h}}$. For the numerical flux $\tilde{\mathcal{F}}_i(\mathbf{U}^l, \mathbf{U}^+, \mathbf{n}_{\mathcal{K}})$ through the faces,

we will take the HLLC flux (see [4]) in the spatial direction and the upwind flux (see [2]) in the time direction.

The shallow water equations are nonlinear and hyperbolic, and hence its solutions may develop or admit discontinuities, such as bores or jumps, from the initial data. To prevent numerical oscillations only around discontinuities, we add a dissipation operator of Jaffre et. al. [1] to the weak formulation (10) and apply wherever the discontinuity detector $\mathcal{I}_{\mathcal{K}}^n$ of Krivodonova et. al. [3] indicates discontinuous regions. The definition of dissipation operator, discontinuity detector and the discretization of weak formulation are presented in Ambati and Bokhove [7]. The resulting discretized equations are then solved by augmenting the equations with a pseudo-time derivative and integrating them until the solution reaches the steady state in pseudo-time (see [7]).

## 4 FLOODING AND DRYING

### 4.1 Free boundary condition

In the finite elements connected to the water font, the mass ($h$) and the momentum ($hu, hv$) at the front must satisfy

$$\mathbf{U}_{\mathsf{h}} = (h, hu, hv)_{\mathsf{h}} = 0 \text{ at } \mathbf{x} \in \Gamma_S. \tag{11}$$

To achieve this boundary condition, we constrain the expansion coefficients of the polynomial approximation $\mathbf{U}_{\mathsf{h}}$. This can be best explained by considering the case in Figure 4.1 in which due to the movement of water front the spatial element $K_{\mathsf{k}}^{n-1}$ has changed into $K_{\mathsf{k}}^n$. Now in the space-time element $\mathcal{K}_{\mathsf{k}}^n$, the face $\mathcal{S}_{\mathsf{m}} := \{G_{\mathsf{k}}^n(\zeta)|\zeta_2 = 1\}$ describes the evolution of water front. To satisfy (11) at the front, we write the polynomial approximation of $\mathbf{U}_{\mathsf{h}}$ at $\zeta_2 = 1$ as

$$\begin{aligned}\sum_m \hat{\mathbf{U}}_{m=0}^7 \hat{\psi}_m =& \hat{\mathbf{U}}_0 + \sum_{m=1}^7 \hat{\mathbf{U}}_m(\hat{\phi}_m - c_m) \\ =& \hat{\mathbf{U}}_0 - \sum_{m=1}^7 \hat{\mathbf{U}}_m c_m + (\hat{\mathbf{U}}_1 + \hat{\mathbf{U}}_6)\zeta_0 + (\hat{\mathbf{U}}_2 + \hat{\mathbf{U}}_4)\zeta_1 + \hat{\mathbf{U}}_3 + (\hat{\mathbf{U}}_5 + \hat{\mathbf{U}}_7)\zeta_0\zeta_1\end{aligned} \tag{12}$$

with $c_m = (\int_{K_{\mathsf{k}}^n} \phi_m \mathrm{d}K)/|K_{\mathsf{k}}^n|$. By adjusting the expansion coefficients of $\mathbf{U}_h$ as

$$\hat{\mathbf{U}}_6 = -\hat{\mathbf{U}}_1,\ \hat{\mathbf{U}}_4 = -\hat{\mathbf{U}}_2,\ \hat{\mathbf{U}}_7 = -\hat{\mathbf{U}}_5 \text{ and } \hat{\mathbf{U}}_3 = -\hat{\mathbf{U}}_0 + \sum_{m=1}^7 \hat{\mathbf{U}}_m c_m \tag{13}$$

we satisfy $\mathbf{U}_h = 0$ for all values of $(\zeta_0, \zeta_1)$ on the face $\mathcal{S}_{\mathsf{m}} := \{G_{\mathsf{k}}^n(\zeta)|\zeta_2 = 1\}$. The adjustment doesn't modify the mean $\hat{\mathbf{U}}_0 = \int_{K_{\mathsf{k}}^n} \mathbf{U}_{\mathsf{h}} \mathrm{d}K$, thus conserving mass $h$ and momentum $(hu, hv)$. Similarly, we can extend this argument for any face of the space-time finite elements.

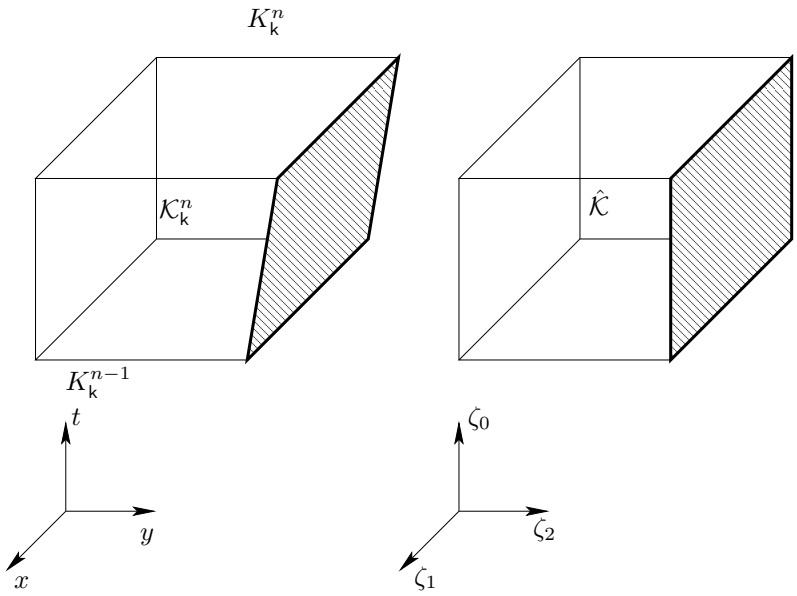


Figure 2: Finite element connected to the water front (left) and the corresponding reference element (right). Shaded region represents the movement of water front in time. The reference element is a cube of size $[-1, 1]^3$.

### 4.2 Free boundary movement

To accomplish the free boundary movement in a restricted case, the flow domain is tessellated with spatial finite elements and then the free boundary edges are identified (see Figure 4.2). The spatial flow domain is now divided into different zones with the parallel grid lines (dotted lines) passing through the free boundary nodes as in Figure 4.2. From the Figure 4.2, we can clearly say that each free boundary edge defines a zone in the grid. We allow the free boundary nodes to move only along the grid lines and thus the zones remain the same in time. Also we identify the nodes in each zone and move them w.r.t the free boundary edge of the zone. Thus, this keeps the size of the elements uniform in the domain and the number of elements and nodes remain the same which is easy to handle. The movement of the interior nodes depend on the movement of free boundary nodes as follows:

$$\Delta x_j = \frac{\Delta x_1 (x_j/x_1)(y_2 - y_j) + \Delta x_2 (x_j/x_2)(y_j - y_1)}{y_2 - y_1}, \tag{14}$$

where $(x_j, y_j)$ are the co-ordinates of the $j^{\text{th}}$ node in the zone of the free boundary with nodes $(x_1, y_1)$ and $(x_2, y_2)$ such that $y_j \in [y_1, y_2]$; $\Delta x_1$ and $\Delta x_2$ is the movement of free boundary nodes obtained either from the exact solutions or by discretizing and solving the front equation (4). The discretization of equation (4) and the level set equation (5) are currently under investigation.

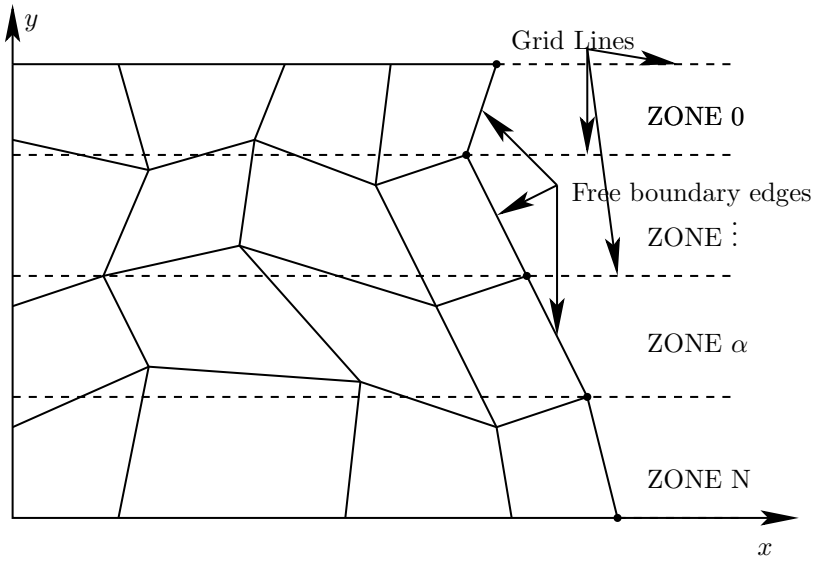


Figure 3: Free boundary edges and its respective zones.

## 5 NUMERICAL RESULTS

### 5.1 Harmonic wave maker

Consider the linearized shallow water equations $\partial_t\eta + H\,(\partial_x u + \partial_y v) = 0$, $\partial_t u + g\partial_x\eta = 0$ and $\partial_t v + g\partial_y\eta = 0$ in a rectangular basin of size $[(0, L_x) \times (0, L_y)]$ with a wave maker at the boundary $x = L_x$, solid walls on the remaining boundaries, $\eta(x, y, t)$ the free surface perturbation around a mean surface $H$, and $(u(x, y, t), v(x, y, t))$ the velocity field. The movement of the wave maker is described as $x = L_x + x_m(y, t)$. Applying the kinematic boundary condition at the wave maker and linearizing the resulting equations, we obtain $\partial_t x_m = u(x = L_x, y, t)$. A linear gravity wave type solution can now be obtained as

$$\begin{aligned}
\eta(x, y, t) &= \eta_0 \cos(kx)\cos(ly)\sin(\omega t),\\
u(x, y, t) &= -\frac{g\,k\eta_0}{\omega}\sin(kx)\cos(ly)\cos(\omega t),\\
v(x, y, t) &= -\frac{g\,l\eta_0}{\omega}\cos(kx)\sin(ly)\cos(\omega t),\ \text{and} \qquad (15)\\
x_m(y, t) &= -\frac{g\eta_0 k sin(kL_x)}{\omega^2}\cos(ly)\sin(\omega t), \qquad (16)
\end{aligned}$$

where $\eta_0$ is the amplitude of the harmonic free surface waves; $A$ the amplitude of the harmonic wave maker; $\omega$ the frequency determined from the dispersion relation $\omega^2 = g\,H\,(k^2 + l^2)$ once $l = n\pi/L_y$ the wave number along $y$ and $k = m\pi/L_x$ the wave number along $x$ are known with $n$ an integer constant and $m$ a real constant.

We initialize the gravity wave solution (15) at $t = 0$, and prescribe the movement of the wave maker at $x = L_x$ using (16) to simulate the waves induced by the wave maker.

To maintain a regular size of the elements, we move the nodes of the grid by linearly interpolating the free boundary movement with the zero movement at the solid wall along $y$. Thus, given the coordinates of a node at time $t_{n-1}$, it is straightforward to determine its position at time $t_n$.

We simulate the non-linear counterparts of the waves generated by the harmonic wave maker from low to high amplitudes. At low amplitude, we see that harmonic waves in the wave maker agrees qualitatively with the solution (15), see Fig. 4(a)-(d) and at high amplitudes, these harmonic waves start to break due to non-linearity and hence, moving bores are formed, see Fig. 5(a)-(d). For low amplitude the energy stays essentially constant, while for high amplitude the energy fluctuates but initially decreases on average due to wave breaking, see Fig. 5.1(a) and (b).

### 5.2 Dam break

Consider the dam break solution of the one dimension shallow water equations:

$$(h,u) = \begin{cases} (h_0, u_0) & \text{if } x < x_0 + (u_0 - \sqrt{gh_0})t \\ \left(\frac{1}{9g}(s - (x-x_0)/t)^2, s - 2\sqrt{gh}\right) & \text{if } x_0 + (u_0 - \sqrt{gh_0})t < x < x_0 + st \\ (0,0) & \text{otherwise} \end{cases} \quad (17)$$

with $(h_0, u_0)$ the initial values of dam break situated at $x = x_0$ and $s = u_0 + 2\sqrt{gh_0}$ the speed of the front after the dam break collapses. We initialize the dam break solution at time $t = t_0 + 0.25$ to avoid the initial discontinuity, and perform the numerical simulation from $t_0 = 0.0$ to 0.1 with $h_0 = 1.0$ and $u_0 = 0.0$. Figure 5.2 shows the numerical and exact solutions of water depth $h$ with the specified front movement in the direction of positive $x$ axis.

### 5.3 Parabolic beach

The one dimensional shallow water equations $\partial_t h + \partial_x(hu) = 0$ and $\partial_t u + u\partial_x u + g\partial_x(h + h_b) = 0$ satisfy (Thacker [**?**])

$$h(x,t) = H - B(x - u_0 \sin(\omega t))^2/2 \text{ and } u(x,t) = u_0 \cos(\omega t) \quad (18)$$

with bottom topography $h_b(x) = Bx^2/2$ in the domain $x \in [-\sqrt{2H/B} + u_0 \sin(\omega t)/\omega, \sqrt{2H/B} + u_0 \sin(\omega t)/\omega]$, where $B = \omega^2/g$, and $u_0$ and $\omega$ are arbitrary parameters. In our nonlinear code, we initialize the parabolic bowl solution (18) at time $t = 0$ in a half domain $[0, \sqrt{2H/B}]$ and simulate by specifying the exact solutions as boundary conditions at the left boundary $x = 0$ and the exact front movement at the right boundary. Figure 18 shows the plots of the water depth $h$ and, run-up and backwash due to the front movement. We also compute $L^2$ error and order of accuracy for various mesh resolution in Table 1.

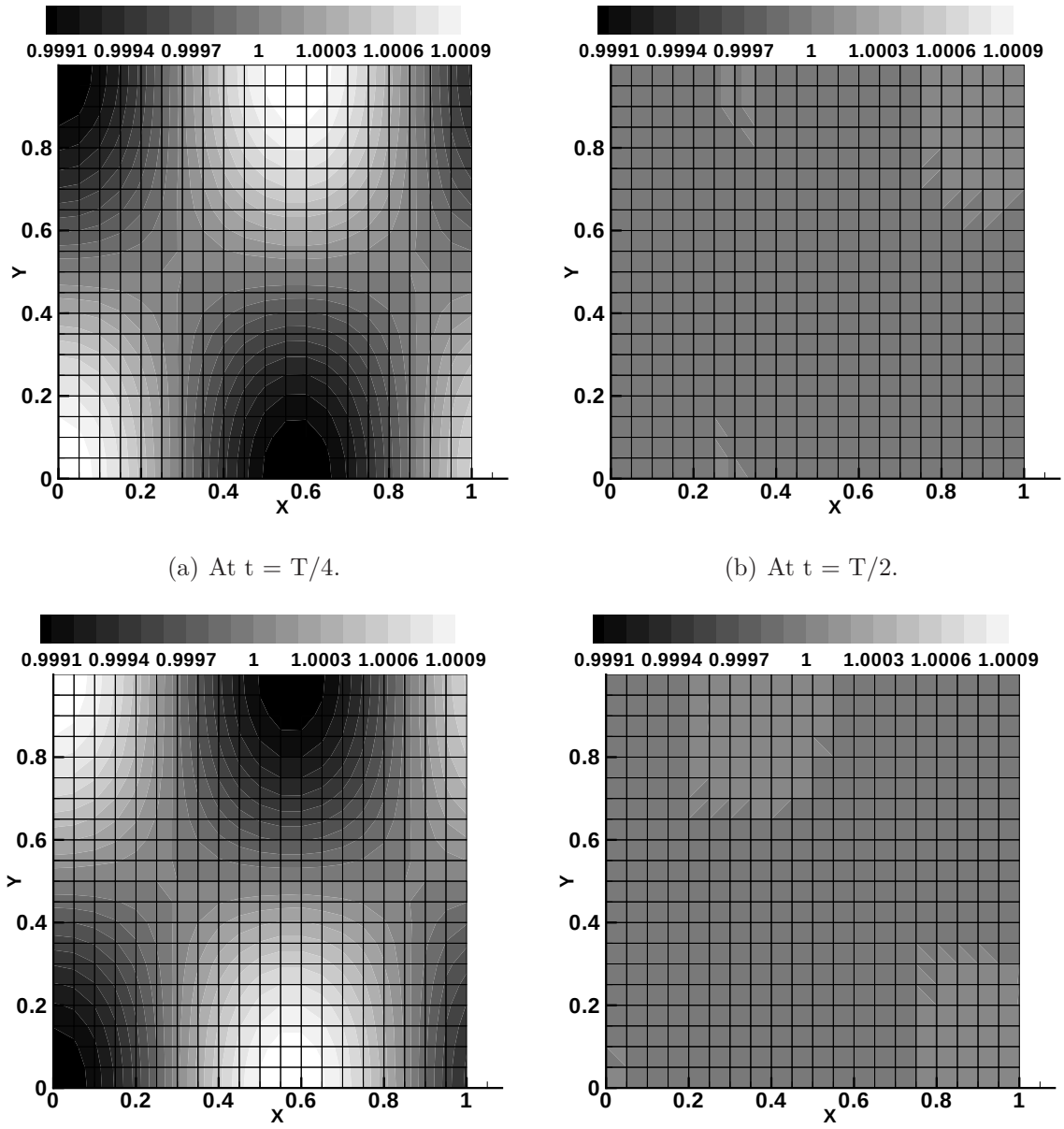


(a) At t = T/4.

(b) At t = T/2.

(c) At t = 3T/4.

(d) At t = T.

Figure 4: Contour plots of water depth $h$ for a time period $T = 2\pi/\omega = 1.0$. Parameters $g = 1$, $H = 1$, $\eta_0 = 0.05$, $n = 1$ and $m = \sqrt{3}$ such that $\omega = 2\pi$.

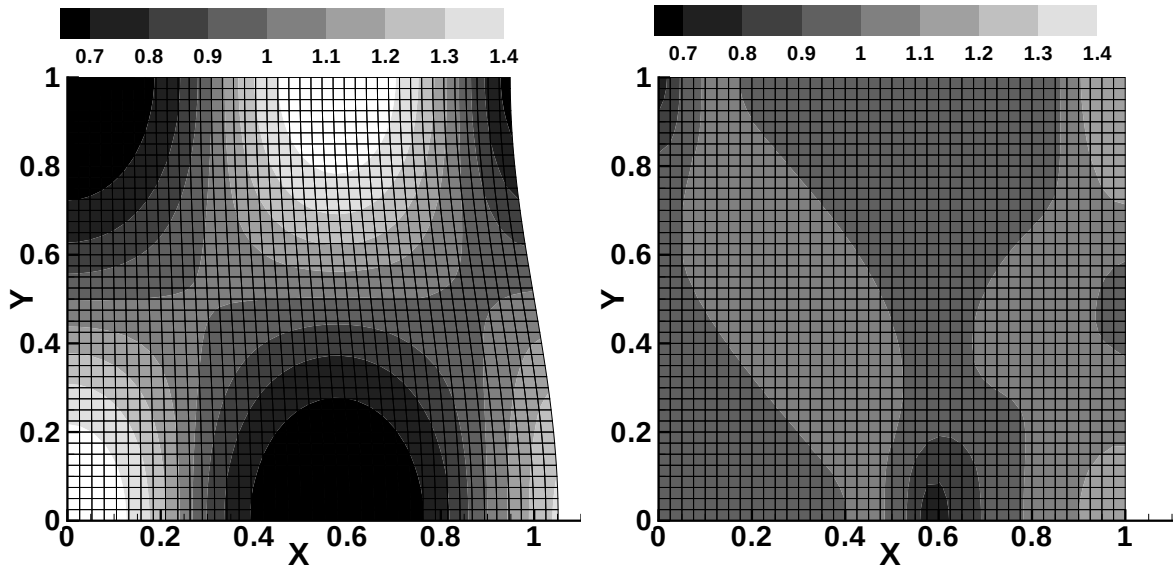


(a) At t = T/4.




(b) At t = T/2.

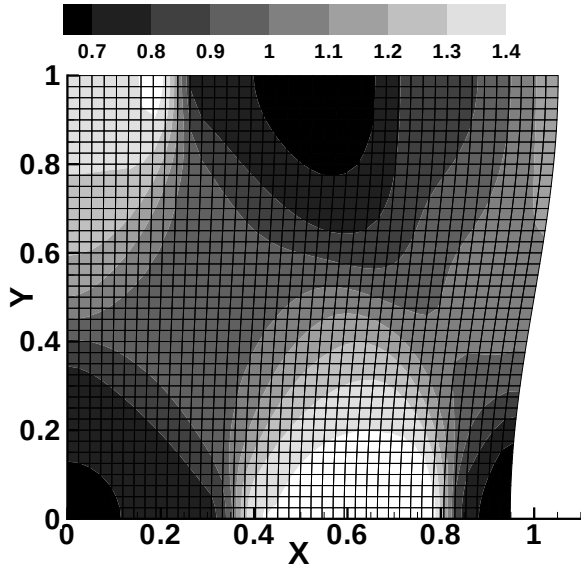


(c) At t = 3T/4.

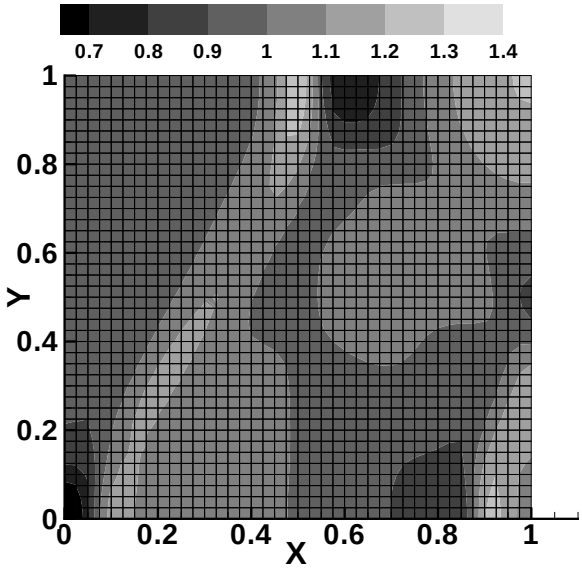


(d) At t = T.

Figure 5: Contour plots of water depth $h$ for a time period $T = 2\pi/\omega = 1.0$. Parameters $g = 1$, $H = 1$, $\eta_0 = 0.05$, $n = 1$ and $m = \sqrt{3}$ such that $\omega = 2\pi$.

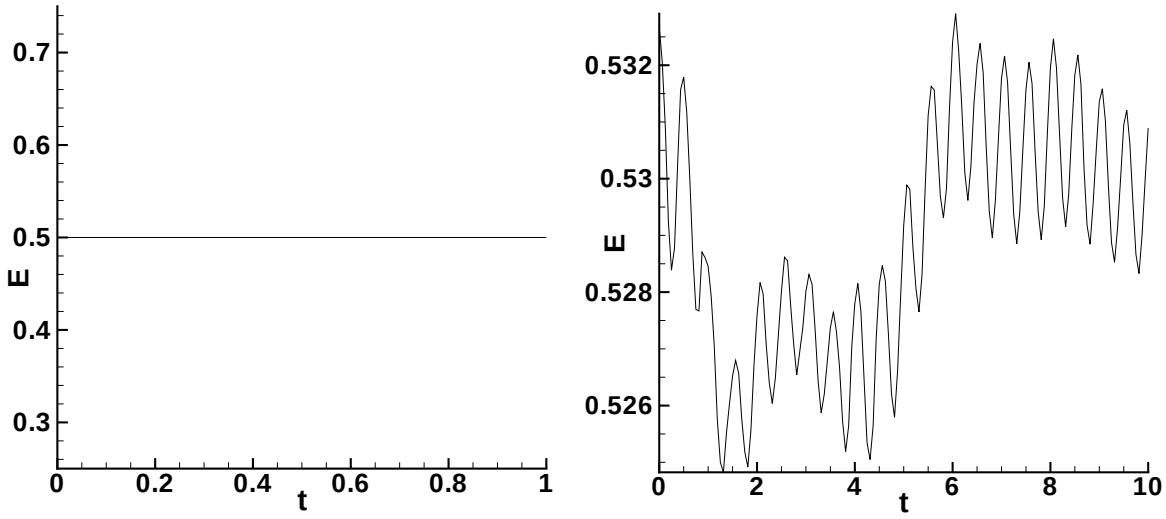


(a) Low amplitude (b) High amplitude

Figure 6: Plots of the energy as a function of time.

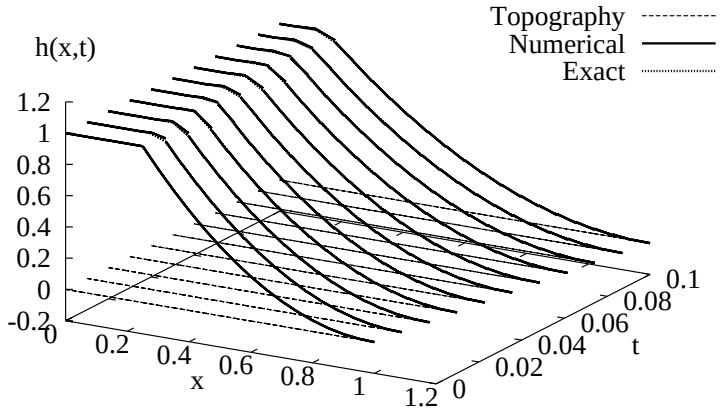


Figure 7: Water depth $h$ of the dam break initialized at $t = 0.25$ and simulated until

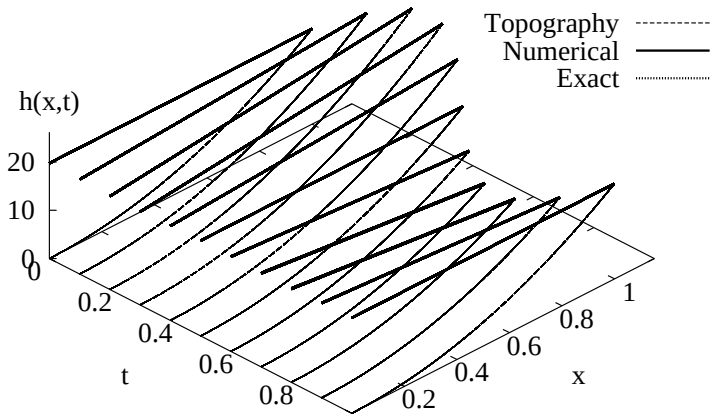


Figure 8: Plots of water depth $h(x,t)$ comparing exact and numerical solutions.

Table 1: $L^2$ error and order of accuracy for $h$ and $hu$.

| For $h$ | | | | | | | |
|---|---|---|---|---|---|---|---|
| $t$ | $10 \times 10$ | $20 \times 20$ | order | $40 \times 40$ | order | $80 \times 80$ | order |
| 0.00 | 1.4713e-02 | 3.6782e-03 | 2.00 | 9.1955e-04 | 2.00 | 2.2989e-04 | 2.00 |
| 0.20 | 5.8917e-02 | 1.0801e-02 | 2.45 | 2.1305e-03 | 2.34 | 4.7273e-04 | 2.17 |
| 0.40 | 6.6478e-02 | 1.4148e-02 | 2.23 | 3.1582e-03 | 2.16 | 8.2114e-04 | 2.12 |
| 0.60 | 6.8447e-02 | 1.3713e-02 | 2.32 | 3.2069e-03 | 2.10 | 7.3023e-04 | 1.89 |
| 0.80 | 3.1554e-02 | 9.1024e-03 | 1.79 | 2.4838e-03 | 1.87 | 6.4977e-04 | 1.93 |
| 1.00 | 7.1911e-02 | 1.5245e-02 | 2.24 | 3.1006e-03 | 2.30 | 6.5842e-04 | 2.24 |
| For $hu$ | | | | | | | |
| 0.00 | 1.4713e-02 | 3.6782e-03 | 2.00 | 9.1955e-04 | 2.00 | 2.2989e-04 | 2.00 |
| 0.20 | 1.6388e-01 | 2.9600e-02 | 2.47 | 6.1817e-03 | 2.26 | 1.4741e-03 | 2.07 |
| 0.40 | 1.9837e-01 | 2.3952e-02 | 3.05 | 2.8370e-03 | 3.08 | 5.4674e-04 | 2.38 |
| 0.60 | 1.1169e-01 | 1.2205e-02 | 3.19 | 1.8580e-03 | 2.72 | 4.1622e-04 | 2.16 |
| 0.80 | 5.6062e-02 | 6.7639e-03 | 3.05 | 1.9006e-03 | 1.83 | 6.4496e-04 | 1.56 |
| 1.00 | 1.7163e-01 | 3.2716e-02 | 2.39 | 5.7802e-03 | 2.50 | 1.0625e-03 | 2.44 |

## 6 CONCLUSIONS AND FUTURE WORK

A space-time discontinuous Galerkin method is discussed for the shallow water equations in time dependent domains. The application of the space-time DG method is novel and it is currently being extended to accurately model the evolution of the water front line in flooding and drying events. These are of tantamount importance in the prediction of river floods and near-shore hydrodynamics.

To show the versatility of the present method in dynamic domains, we considered the generation of nearly linear and highly nonlinear waves by prescribing the motion of a flexible domain wall as a wave maker. Further, the ability of method to deal with flooding and drying is demonstrated numerically by considering some exact solutions, where the exact front movement is specified in the numerical code. However, we are currently extending this method for the physical evolution of the free boundary movement.

## REFERENCES

[1] J. Jaffre, C. Johnson, A. Szepessy, Convergence of the discontinuous Galerkin method for hyperbolic conservation laws, *Math. Models and Methods in Appl. Sci.,* **5** 367–386 (1995).

[2] J.J.W. Van der Vegt, H. Van der Ven, Space-time discontinuous Galerkin finite element method with dynamic grid motion for inviscid compressible flows, *J. Comput. Phys.* **182** (2002) 546-585.

[3] L. Krivodonova, J. Xin, J.-F. Remacle, N. Chevaugeon, J.E. Flaherty, Shock detection and limiting with discontinuous Galerkin methods for hyperbolic conservation laws, *Appl. Numer. Math.,* **48** 323–338 (2004).

[4] O. Bokhove, Flooding and drying in finite-element Galerkin discretizations of shallow-water equations. Part I: One dimension. *J. Sci. Comput.*, **22**, 47–82, (2005). http://www.math.utwente.nl/∼bokhoveo

[5] S. Osher and R. Fedkiw, *Level set methods and dynamic implicit surfaces*, Springer-Verlag, New York, (2003).

[6] V.R. Ambati and O. Bokhove, Space-time discontinuous Galerkin finite element method for shallow water flows. *J. Comput. Appl. Math.,* accepted, (2006). http://www.math.utwente.nl/∼ambativr

[7] V.R. Ambati and O. Bokhove, Space-time discontinuous Galerkin discretization of rotating shallow water flows on moving grids. *submitted to J. Comput. Phys.,* (2006). W.C. Thacker, Some exact solution to the nonlinear shallow-water wave equations, *J. Fluid Mech.,* 107, 499–508, (1981).

[8] W.E.H. Sollie, J.J.W. van der Vegt and O. Bokhove, A discontinuous Galerkin finite element method for two fluid flow, Part I: one space dimension. *submitted to J. Comput. Phys.*, (2006).